Environmental Science & Technology

pubs.acs.org/est

Article

2D N-Doped Porous Carbon Derived from Polydopamine-Coated Graphitic Carbon Nitride for Efficient Nonradical Activation of Peroxymonosulfate

Jie Miao, Wei Geng, Pedro J. J. Alvarez, and Mingce Long*

Cite This: *Environ. Sci. Technol.* 2020, 54, 8473−8481

Read Online

ACCESS | Metrics & More | Article Recommendations | Supporting Information

ABSTRACT: Nitrogen-doped carbon materials attract broad interest as catalysts for peroxymonosulfate (PMS) activation toward an efficient, nonradical advanced oxidation process. However, synthesis of N-rich carbocatalysts is challenging because of the thermal instability of desirable nitrogenous species (pyrrolic, pyridinic, and graphitic N). Furthermore, the relative importance of different nitrogenous configurations (and associated activation mechanisms) are unclear. Herein, we report a "coating-pyrolysis" method to synthesize porous 2D N-rich nanocarbon materials (PCN-*x*) derived from dopamine and g-C_3N_4 in different weight proportions. PCN-0.5 calcined at 800 °C had the highest surface area (759 m^2/g) and unprecedentedly high N content (18.5 at%), and displayed the highest efficiency for 4-chlorophenol (4-CP) degradation via PMS activation. A positive correlation was observed between 4-CP oxidation rates and the total pyridinic and pyrrolic N content. These N dopants serve as Lewis basic sites to facilitate 4-CP adsorption on the PCN surface and subsequent electron-transfer from 4-CP to PMS, mediated by surface-bound complexes (PMS−PCN-0.5). The main degradation products were chlorinated oligomers (mostly dimeric biphenolic compounds), which adsorbed to and deteriorated the carbocatalyst. Overall, this study offers new insights for rational design of nitrogen-enriched carbocatalysts, and advances mechanistic understanding of the critical role of N species during nonradical PMS activation.

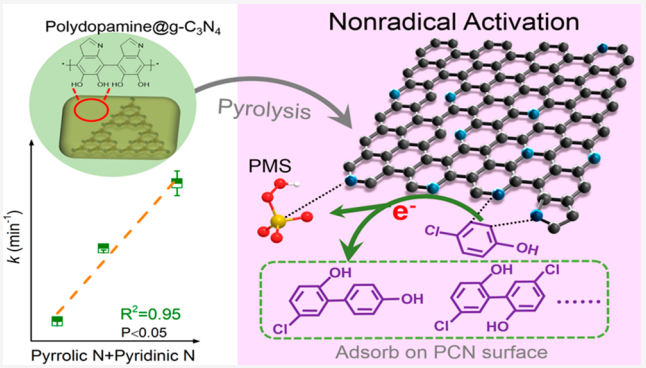

INTRODUCTION

Persulfate based advance oxidation processes (AOPs) show superior oxidation efficiency in the removal of refractory organic contaminants.[1−3] Unlike most metal oxide-catalyzed persulfate activation that produces radicals,[4] carbocatalysts trigger nonradical activation of persulfate, which is less susceptible to interference (e.g., radical scavenging) by nontarget compounds in complex water matrices, and does not release toxic metals.[5−8] The mechanism for nonradical persulfate activation by carbocatalysts is frequently ascribed to singlet oxygenation or mediated electron-transfer.[9,10] However, the relative importance of these potential nonradical pathways is debatable.

Carbocatalysts including graphene,[5] nanodiamonds,[7] carbon nanotubes (CNT),[8] and mesoporous carbon[11] have been investigated for persulfate activation, but they showed marginal performance.[5,12] N doping, can improve the catalytic activity of carbocatalysts by tailoring their surface chemical properties, modulating the electron distribution (electronegativity: χ_N = 3.04 > χ_C = 2.55) in the carbonaceous framework, and creating more charged active sites.[13−20] Generally, the introduced N functionalities (such as pyrrolic, pyridinic, and graphitic N) can serve as active sites and contribute to the enhanced catalytic performance.[21−25] Although the role of N-dopants on PMS activation has not been completely elucidated, pyridinic N (sp^2 hybridized N containing 6-membered ring) and pyrrolic N (sp^2 hybridized N containing 5-membered ring) are known Lewis bases that could serve as adsorption sites on the carbonaceous framework for electrophilic molecules like peroxymonosulfate (PMS) and phenolic compounds,[6,23,26] possible facilitating redox reactions. Furthermore, the content of graphitic N was positively correlated with catalytic activity due to the enhanced conductivity and facilitated electron transfer.[19,21]

The deliberate design of N-rich carbocatalysts is conducive to creating active sites toward high catalytic capability in persulfate activation and to discern the role of N species. As

Received: May 19, 2020
Accepted: June 8, 2020
Published: June 8, 2020

https://dx.doi.org/10.1021/acs.est.0c03207
Environ. Sci. Technol. 2020, 54, 8473−8481

one of the most N-rich precursors, graphite carbon nitride (g-C_3N_4 with 57.1 at% of N contents) is used to prepare N-doped graphene (NG) and other N doped carbon.[27−31] However, the required calcination temperatures are well above the decomposition temperature (710 °C) of g-C_3N_4, thereby leading to significant N loss.[28] An efficient NG electrocatalyst was previously obtained by direct annealing of g-C_3N_4 at 900 °C in a special homemade container to inhibit excessive N loss, but the retained N content was quite low (5.4 at%) and a limited number of N species (only pyridinic N and graphitic N) were introduced.[29] In separate work, N-rich carbon nanosheets (11.6 at%) were synthesized by the pyrolysis of g-C_3N_4 template coated with carbonized glucose via hydrothermal treatment,[28] which provided a means to control N contents. However, this approach suffers from time-consuming and complex synthesis steps. Hence, it is still a challenge to obtain g-C_3N_4-derived carbon with high N content and tunable nitrogenous forms.

Herein, we report a facile and feasible strategy ("coating-pyrolysis") to synthesize porous N-doped carbon nanosheets (PCN) with an unprecedently high N content (up to 18.5 at% at 800 °C), using g-C_3N_4 as the template and polydopamine (PDA) as the coating. PDA, a polymer with rich pyrrolic-N groups obtained by self-polymerization of dopamine (DA) under mild alkaline conditions, was selected as a supplemental nitrogen source and as a tight coating on g-C_3N_4 to suppress N loss.[32−34] Activity enhancement by the presence of nitrogen was corroborated by a positive correlation between the total contents of pyridinic and pyrrolic N versus the oxidation rates of 4-chlorophenol (4-CP) in PCN/PMS systems.

EXPERIMENTAL SECTION

Chemical Reagents. Phenol, 4-CP, bisphenol A (BPA), 2,4-dichlorophenoxyacetic acid (2,4-D), benzoic acid (BA), ibuprofen, *p*-chloroaniline (*p*-CA), *p*-benzoquinone (*p*-BQ), *tert*-butyl alcohol (TBA), methanol (MeOH), furfuryl alcohol (FFA), potassium iodide (KI), sodium sulfate (Na_2SO_4), hydrogen peroxide (H_2O_2, 30%), persulfate (PDS), and Oxone ($2KHSO_5{\cdot}KHSO_4{\cdot}K_2SO_4$) are all analytical grade reagents and were purchased from Sinopharm Chemical Reagent Co., Ltd. 5,5-Dimethyl-1-pyrroline-N-oxide (DMPO, 98%) and 2,2,6,6-tetramethyl-4-piperidinyl (TEMP, 99%) were purchased from Aladdin (Shanghai). DCD and DA were used as source materials.

Preparation of Porous N-doped Carbon (PCN). Metal-free PCN catalysts with different N contents were synthesized through a coating-pyrolysis process. Briefly, DCD (5 g) was transferred into a 50 mL ceramic crucible with a lid; then, heated to 550 °C (5 °C min^{-1}) and kept for 4 h in a muffle furnace. The yellow residual was ground to obtain g-C_3N_4. Next, 0.5 g of g-C_3N_4 was dispersed in a 40 mL DA aqueous solution. The mixture was magnetically stirred for 5 min; then, polymerization was performed by adding 3.1 mL $NH_3{\cdot}H_2O$ (0.9 M) and keeping the mixture stirring at 25 °C for 2 h. The C_3N_4@PDA hybrids were obtained after washing with water and drying at 60 °C for 12 h. The morphologies of g-C_3N_4 and C_3N_4@PDA hybrids are shown in Figure S1 of the Supporting Information (SI). After that, the as-prepared C_3N_4@PDA hybrids were placed in a homemade quartz tube (ϕ24 × 6 × L200 mm^3) with a piston (ϕ17 × L50 mm^2) and carbonized at 800 °C for 2 h under a high-purity argon flow (80 mL min^{-1}). The obtained samples were named PCN-*x*, where *x* is the mass ratio (*x* = 0.5, 1, and 1.5) of DA to g-C_3N_4. The sample with a ratio less than 0.5 was also tried but the yield of the product is negligible due to the inherent volatility of g-C_3N_4 at a temperature over 710 °C.[28] The characterization of PCN-*x* catalysts is described in Text S1.

Activity Evaluation. The catalytic activity of catalysts was evaluated by 4-CP oxidation in PMS-based AOPs, and the detailed degradation process is shown in Text S2. To investigate the selective oxidation performance of PCN/PMS system, degradation of selective organic pollutants was tested, and their concentrations were analyzed on a Shimadzu LC-2010AHT high-performance liquid chromatography (HPLC). The detailed analytical conditions of HPLC were listed in Table S1. The apparent reaction first-order rate constants for the degradation of all organic compounds were determined by data fitting.

The concentrations of PMS and PDS were both detected by a 2,2′-azino-bis (3-ethylbenzothiazoline-6-sulfonic acid) diammonium salt (ABTS) method.[35] In the recycle tests, the used catalyst was recovered, washed, and dried for the second test. After the second run, the collected catalyst was regenerated by using MeOH as an extracting reagent to remove the lipophilic degradation products. The process was performed in an ice bath with the assistant of ultrasound.

Statistical Analysis. All kinetic experiments were conducted in triplicate, and standard deviations from the mean were presented. The error values verified that all experiments are replicable. Student's paired *t* test (single-tailed) was used to evaluate the significance of the differences between treatments at the 95% confidence level ($p < 0.05$).

RESULTS AND DISCUSSION

Characterization of PCN-*x* Catalysts. Metal-free nitrogen-doped carbon catalysts were synthesized by the pyrolysis of C_3N_4@PDA hybrids, and the PDA coating was formed by mixing g-C_3N_4 with various amounts of DA in an ammonia solution (0.9 M) (Figure 1a). As shown in SEM and TEM images (Figure 1b,c), the as-synthesized PCN features smooth 2D nanosheet structures. Figure 1d shows the high-resolution TEM (HRTEM) image of the selected-area in Figure 1c; the

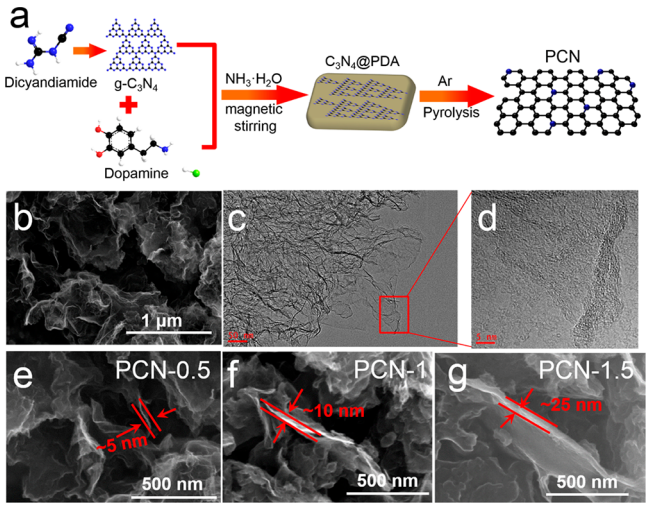

Figure 1. (a) Fabrication of the PCN following a coating-pyrolysis route (red atom-O, black atom-C, blue atom-N, white atom-H, green atom-Cl); (b) SEM image; (c, d) HRTEM images of PCN-0.5; (e−g) SEM images of PCN-0.5, PCN-1, and PCN-1.5, respectively.

https://dx.doi.org/10.1021/acs.est.0c03207
Environ. Sci. Technol. 2020, 54, 8473−8481

legible fringes appear at the edges of the samples, indicating partial graphitization of PCN after carbonization. The SEM images in Figure 1e−g show that nanosheet thicknesses of PCN-0.5, PCN-1 and PCN-1.5 are ∼5, ∼10, and ∼25 nm, respectively. The thickness of catalysts increases with the increase of DA dosages. Furthermore, specific surface areas (SSAs), average pore sizes, and pore volumes of PCN catalysts (listed in Table S2) were estimated by N_2 adsorption−desorption profiles (Figure S2). All PCN catalysts have the type IV isotherm of hysteresis loops, suggesting the existence of mesopores.[27,32] Pore size distributions presented in the inset of Figure S2 indicate the pore sizes centering at 2.4−5.5 nm. Table S2 shows that the SSA decreases from 759 $m^2\ g^{-1}$ (PCN-0.5) to 196 $m^2\ g^{-1}$ (PCN-1.5) with an increase in the DA content. Nevertheless, mesoporous structures of PCN can provide more active sites and facilitate the adsorption of pollutants during catalytic oxidation.

Generally, DA has a significant influence on the yield of the final powder (PCN-*x*) because the PDA coating can suppress both the volatilization of g-C_3N_4 and the loss of nitrogen during calcination. As shown in Figure 2a, the yield of PCN

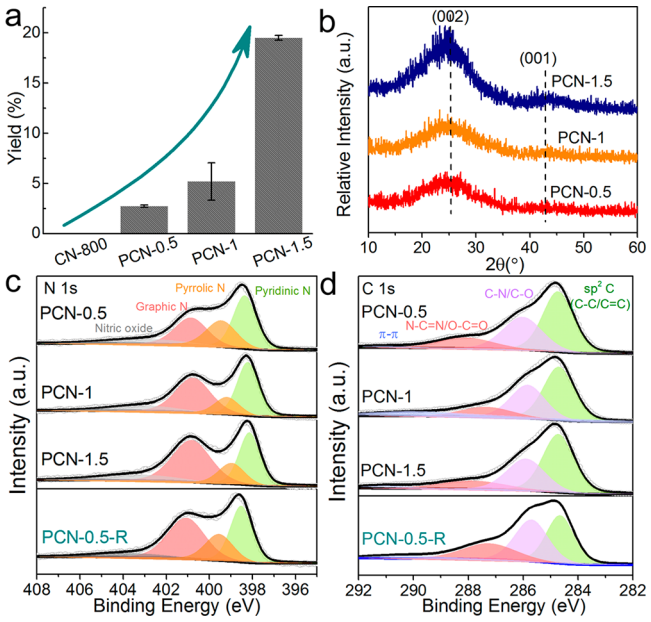

Figure 2. (a) Production yields of different PCN samples; (b) XRD patterns of PCN-*x* (*x* = 0.5, 1, 1.5); XPS spectra of PCN-*x* and PCN-0.5 after reaction (PCN-0.5-R), (c) N 1s, and (d) C 1s.

can be improved by an increase in the DA dose (i.e., the PCN-*x* (*x* = 0.5, 1, 1.5) yield was 2.8%, 5.18%, and 19.5%, respectively). XRD patterns (Figure 2b) and Raman spectra (Figure S3a) show the structural evolution of PCN-*x* during synthesis. The observed broad peaks at around 25° and weak peaks at 43° in Figure 2b correspond to the (002) and (001) planes of the graphitized structures, respectively. The low intensity and large full width at half-maximum (fwhm) indicate a low degree of crystallinity of PCN catalysts. Besides, as shown in Figure S4, the slightly stronger intensity of the two peaks with an increase in calcination temperature demonstrates an improvement in the degree of graphitization. The XRD pattern of PCN-1 obtained at 700 °C shows an obvious broad peak corresponding to (002) plane of graphitic carbon (Figure S5), while CN prepared by the pyrolysis of the pristine g-C_3N_4 at 700 °C still retains the original tri-s-triazine and conjugated aromatic structures, which respectively correspond to (100) and (002) planes.[36] This result suggests that PDA coating on g-C_3N_4 enables the carbonization of C_3N_4@PDA at lower calcination temperatures. Raman spectra of PCN-*x* samples in Figure S3 display two typical D and G bands roughly at 1350 and 1580 cm^{-1}, respectively. Their intensity ratios (I_D/I_G) are used to evaluate the proportion of defects and disordered structures in carbon materials.[25] Here, I_D/I_G values increased from 1.04 (PCN-0.5) to 1.08 (PCN-1.5), indicating less defects in bulk PCN generated with the increasing N contents, due to a modified carbon framework by the doped nitrogen atoms.[37]

XPS measurements were performed to confirm the elemental compositions and surface chemical states of PCN catalysts. XPS survey spectra in Figure S6 illustrate the presence of C, N, and O on the surface of all PCN samples (top few nm). Additionally, Table S3 lists the relative atom contents. As the DA dose increases, the surface N dopants decrease from 18.5% (PCN-0.5) to 15.7% (PCN-1.5). This trend can be attributed to the dilution effect of PDA, which has much lower N content than g-C_3N_4. The nitrogen chemical status on the surface of PCN catalysts was further analyzed by N 1s spectra (Figure 2c). The four deconvoluted peaks respectively correspond to pyridinic N (398.3 eV), pyrrolic N (399.5 eV), graphitic N (400.9 eV), and nitrogen oxides (403.2 eV).[38,39] Among them, nitrogen oxides have been demonstrated to be ineffective for catalytic activity of carbocatalysts.[5] The quantification of these N species is summarized in Table 1. Overall, the contents of pyridinic N and pyrrolic N increased significantly by increasing the N amounts in PCN-*x*, while graphitic N amounts show a slightly downward trend. More importantly, PCN-0.5 exhibits the highest contents of pyridinic N (6.85 at%) and pyrrolic N (4.49 at%) among all the PCN-*x* samples. Furthermore, the contents of C species were quantified by fitting C 1s spectra (Figure 2d), and results are shown in Table S4. The content of two-carbon species, sp^2 C (C−C/C═C) (284.7 eV) and C−O (286.0 eV), increase gradually with the increasing DA amount, which are the dominated C species in all the samples. Conclusively, PCN-0.5 possesses the thinnest nanosheet, the highest N content, the highest SSA, and the most abundant porous structure.

PCN-*x* Catalytic Performance for PMS Activation. The catalytic activity of PCN-*x* carbon nanosheets for PMS activation should be enhanced by large SSA, abundant defects,

Table 1. Relative Amounts of N Species on the PCN Catalysts

	content of N species in N 1s (At%)			
samples	graphitic C (%)	pyridinic N (%)	pyrrolic N (%)	nitric oxide (%)
PCN-0.5	5.02	6.85	4.49	2.15
PCN-1	6.66	6.34	2.31	2.04
PCN-1.5	6.76	4.65	2.31	1.96

https://dx.doi.org/10.1021/acs.est.0c03207
Environ. Sci. Technol. 2020, 54, 8473−8481

and high N content. The oxidation of 4-CP was used to evaluate the catalytic performance of PCN-*x*. In Figure 3a, only

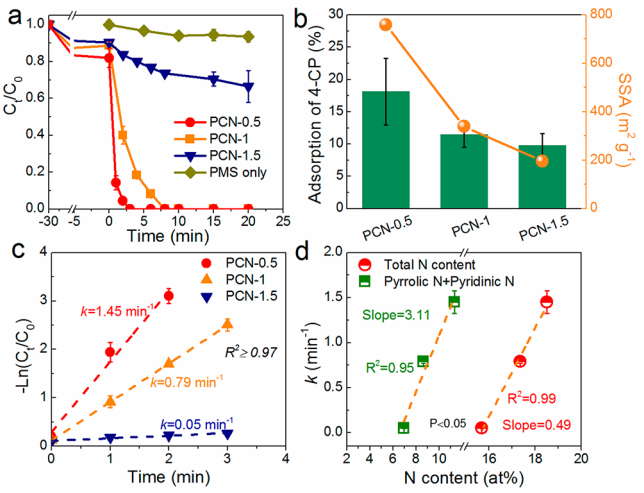

Figure 3. (a) Degradation of 4-CP in PMS-based AOPs catalyzed by different PCN catalysts; reaction conditions: $[PMS]_0$ = 1 mM, C(4-CP)$_0$ = 20 mg L^{-1}, C(catalyst) = 0.05 g L^{-1}, T = 25 °C, initial pH = 6.81. (b) Relationship of different adsorption capacity and the special areas (SSA) of PCN-*x*; (c) first-order kinetics of 4-CP degradation in PCN/PMS systems; and (d) correlations between N content or pyrrolic N + pyridinic N, respectively, versus reaction rate constants.

0.9% 4-CP was directly oxidized by PMS within 20 min in the absence of catalysts, whereas PCN-*x* effectively catalyzed PMS decomposition for rapid 4-CP oxidation. The effect of calcination temperature on the catalytic activity of PCN-*x* catalysts (PCN-1) in PMS system was investigated (Figure S7). Compared to PCN-1−700 (35%) and PCN-1−800 (83%), both PCN-1−900 and PCN-1−1000 catalyzed a very high 4-CP removal efficiency (100%) within 4 min. This result may be attributed to the increased amount of graphitic structures with the increase of calcination temperatures, which is in favor of electron-transfer, and accordingly promotes 4-CP removal.[15,40,41] Nevertheless, due to the poor thermal stability of pyridinic N and pyrrolic N, a high pyrolysis temperature can result in less tunable N species and a decreased N-doping level.[26,28] Therefore, to ensure high N contents and diverse N species, all PCN-*x* in the following sections were obtained at the 800 °C to investigate the role of the nitrogen contents and species on the catalytic activity for PMS activation.

Figure 3b shows that PCN-*x* catalysts displayed a notable adsorption for 4-CP, most likely due to their large SSAs and abundant mesoporous structures. Removal of 4-CP by adsorption increases from 9.8% (PCN-1.5) to 18.1% (PCN-0.5). As observed in Figure 3a, all the PCN-*x* exhibit significant catalytic activity for 4-CP removal in the PMS system. The apparent reaction rate constants (k) for these PCN-*x* catalysts were then calculated by fitting the first-order kinetics (Figure 3c). The rate constants for PCN-0.5 (1.45 min^{-1}) and PCN-1 (0.79 min^{-1}) were 29- and 15.8-fold higher than that for PCN-1.5 (0.05 min^{-1}). Both SSA and total N content were positively correlated with k values for PCN-*x*, with stronger correlations for the latter (R^2 = 0.99 vs 0.81). PCN-0.5 with the highest N contents exhibited the highest catalytic performance (Figure 3d). These results indicate that N content plays a more significant role than SSA in enhancing the catalytic performance of PCN catalysts to activate PMS for 4-CP removal.

Although nitrogen doping has been reported to boost the catalytic activity of carbon catalysts by creating more active sites and tuning electron density,[5,19] the mechanistic roles of pyridinic N, pyrrolic N, or graphic N on N-doped carbon are not fully understood.[42−44] Figure S8 shows that the contents of both pyrrolic N and pyridinic N separately show a positive linearity with activity (k) of PCN-*x* catalysts, indicating that they are beneficial to PMS activation. Note that the R^2 (0.86) value and slope (0.59) for pyridinic N are higher than for pyrrolic N (R^2 = 0.53, slope = 0.47), suggesting that pyridinic N might be the predominant active sites in PCN-*x*/PMS systems. Nevertheless, the total pyridinic plus pyrrolic N content has a stronger linearity and positive correlation with k values than the separate N content categories (Figure 3d). This highlights the importance to consider the summation of pyridinic and pyrrolic N in PCN-*x* for PMS activation since both N species are Lewis basic sites that improve the adsorption of electrophilic compounds (like oxidants and phenolic compounds) on the PCN surface.[26,39] Note that the correlation between the total N contents and k values is stronger, indicating that the role of graphitic N should not be ignored. Graphitic N can improve the conductivity of carbocatalysts, and accordingly promote electronmigration and PMS activation.[19,26] Overall, compared to other PCN-*x* catalysts, the high catalytic activity of PCN-0.5 for PMS activation can be ascribed to its larger SSA, abundant porous structure, and higher N content (especially the summation of pyridinic and pyrrolic N).

The effect of oxidants (PMS, PDS, and H_2O_2) on the catalytic activity of PCN-0.5 was also investigated. PCN-0.5 exhibits a slightly higher catalytic performance with PMS than with PDS activation, with 100% removal efficiency of 4-CP in both cases but 37% (PCN-0.5/PDS) versus 45% (PCN-0.5/PMS) TOC removal within 20 min (Figure S9a). This was attributed to the difficulty in breaking O−O bonds in a symmetrical structure like PDS molecules.[3] H_2O_2 cannot be activated by PCN-0.5, may be due to the stronger bond energy of O−O in H_2O_2 than that in persulfate and a poor affinity toward the catalyst (Table S5). Figure S9b shows the consumption of persulfates in these reactions. In the absence of 4-CP, PMS was consumed only 28.2% within 20 min. However, PMS decomposition increases in the presence of 4-CP, with more than 38% PMS reduction within 20 min. A similar trend also appears in the consumption of PDS. This indicates that there is a direct interaction between the catalyst and persulfate (e.g., nonradical PMS−PCN-0.5 complex), and 4-CP can serve as an electron donor to promote the conversion of persulfate (an electron-transfer process happened and PCN-0.5 as an electron mediator).

The effects of temperature and pH on 4-CP removal in PCN-0.5/PMS system were also investigated. As shown in Figure S10a, high temperature promoted 4-CP removal. According to the Arrhenius equation, the activation energy (E_a) of PCN-0.5 was 24.93 kJ mol^{-1}, which is lower than that reported for N-modified carbon catalysts such as NGC (30.0 kJ mol^{-1}),[45] N-rGO (31.6 kJ mol^{-1}),[46] and N-CNT (36.0 kJ mol^{-1}).[47] The low activation energy may be the reason for the efficient reaction of PCN-0.5/PMS system. Furthermore, Figure S10b presents the effect of initial pH below 9.5 to avoid the PMS activation under alkaline conditions. Although pH decreased significantly (generally below pH 3.5) after adding PMS (Table S6), there was no significant difference for 4-CP removal efficiency over a wide range of initial pH (3.4−

https://dx.doi.org/10.1021/acs.est.0c03207
Environ. Sci. Technol. 2020, 54, 8473−8481

8.2), and only a slight decrease in 4-CP degradation was observed at initial pH = 9.2 (which decreased to pH 3.7). This could be explained by the pH-dependent PCN-0.5 surface charges. Zeta potential values of PCN-0.5 were positive below pH 3.5 (inset of Figure S10b), suggesting the surface of PCN-0.5 is positively charged at pH < 3.5 due to the protonation of electronic rich N and unsaturated C atoms.[48] When the reaction pH was above 3.5 (e.g., pH = 3.7 for treatment with initial pH = 9.2), the electrostatic repulsion would hinder the affinity of both 4-CP (pK_a = 9.43) and PMS (pK_a = 9.40) toward the PCN-0.5 surface,[49,50] resulting in decreased generation of surface PCN−PMS active complexes (as demonstrated below) and passivated degradation of 4-CP. Overall, PCN-0.5/PMS systems exhibit effective performance over a wide initial pH range, which is important for water treatment applications.

PMS dosages above 0.5 mM showed no significant effect on 4-CP removal (Figure S10c). This indicates a high utilization efficiency of PMS in the PCN-0.5/PMS system, so that 0.5 mM PMS is almost enough for efficient degradation of 4-CP. Previous radical based PMS activation results indicated that the removal of organic pollutants would be obviously promoted by increasing PMS concentration and excessive PMS will consume reactive radicals and drops the removal efficiency.[51] The different results of the PCN-0.5/PMS system suggests that it may be an efficient nonradical based AOPs, which is demonstrated in the following section.

Mechanism for Nonradical Activation of PMS. N-doped carbon is known to catalyze nonradical based PMS activation for organic oxidation,[5] but it is still unclear whether the predominant mechanism involves oxidation by singlet oxygen or mediated electron-transfer processes. Thus, the quenching tests using specific scavengers were conducted to discern the generated reactive species and advance understanding of the activation mechanism in the PCN-0.5/PMS system. MeOH ($k(^{\bullet}OH)$ = 9.7 × 10^8 M^{-1} s^{-1} and $k(SO_4^{\bullet-})$ =3.2 × 10^6 M^{-1} s^{-1})[52] and TBA ($k(^{\bullet}OH)$ = 7.6 × 10^8 M^{-1} s^{-1})[33] were selected as radical quenchers. Addition of the two scavengers showed no inhibition of 4-CP removal (Figure 4a), indicating the insignificant role of radicals in this treatment system.

FFA was used as a scavenger for singlet oxygen ($^1O_2$) due to its much higher reaction rate ($k(^1O_2)$ = 1.2 × 10^8 M^{-1} s^{-1}) than 4-CP ($k(^1O_2)$ = 6.0 × 10^6 M^{-1} s^{-1}).[53] However, addition of FFA (0.75 mM) resulted in only slightly suppressed removal of 4-CP. Moreover, FFA alone had a poor removal efficiency (only 10% within 15 min), which is much lower than that of 4-CP alone (Figure S11). This suggests that $^1O_2$ does not play a significant role in this system. Furthermore, the degradation of additional organic pollutants was demonstrated in the PCN-0.5/PMS system (Figure S12a). BA was known as an indicator of free radicals due to its distinct reaction rate constants for $^{\bullet}OH$ (k(BA, $^{\bullet}OH$) = 4.2 × 10^9 M^{-1} s^{-1}) and $SO_4^{\bullet-}$ (k(BA, $SO_4^{\bullet-}$) = 1.2 × 10^9 M^{-1} s^{-1}).[54] However, the degradation of BA (k = 0.002 min^{-1}) was negligible (Figure S12b), reconfirming the absence of $SO_4^{\bullet-}$ and $^{\bullet}OH$ in this system due to the high sensitivity of BA toward radicals. Ibuprofen and 2,4-D were also resistant to degradation. In contrast, other phenolic compounds (such as phenol, and BPA) and P-CA were eliminated within 5 min. This indicates the selective reactivity of this nonradical reaction. BPA was reported to be passively oxidized by $^1O_2$,[53,54] while it was efficiently removed

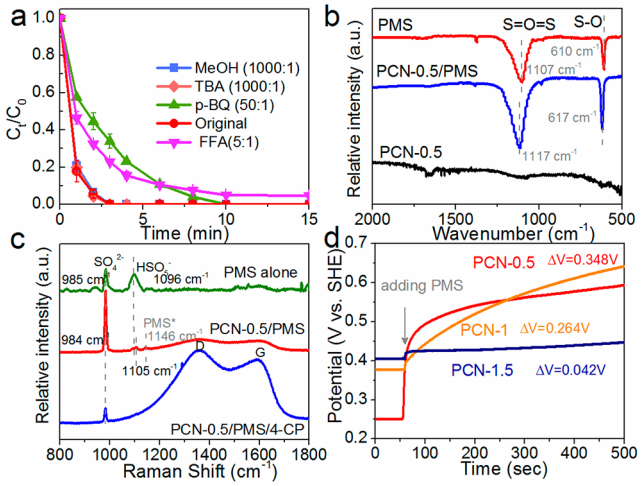

Figure 4. (a) Quenching tests by using different free radical scavengers during 4-CP removal; Reaction conditions: $[PMS]_0$ = 1 mM, $C(4\text{-CP})_0$ = 20 mg L^{-1}, [PCN-0.5] = 0.05 g L^{-1}, T = 25 °C, initial pH = 6.81; (b) in situ FTIR spectra of PCN-0.5, PMS alone, and PCN-0.5 combined with PMS; (c) in situ Raman spectra of PMS alone, PCN-0.5/PMS, and PCN-0.5/PMS/4-CP; and (d) the changes of open-circuit potentials of PCN-x-PMS complexes.

in the PCN-0.5/PMS system, proving the oxidation is not dominated by $^1O_2$ again.

EPR tests were then conducted to further investigate this nonradical mechanism. DMPO and TEMP were individually used as the spin trap of radicals and $^1O_2$.[55,56] As seen in Figure S13a, no obvious signal appeared when DMPO was added in PCN-0.5/PMS system. This confirms the absence of radicals ($^{\bullet}OH$ and $SO_4^{\bullet-}$) in this system. However, a noticeable characteristic signal of TEMP−$^1O_2$ adducts with a three-line pattern[56] was detected. The $^1O_2$ evolution during 4-CP degradation was tracked in Figure S13b. Regardless of the presence of contaminants, $^1O_2$ formation rate had no correlation with the removal rate of 4-CP, which corroborates the minor role of $^1O_2$ in the reaction.

In situ FTIR and Raman analyses were conducted to observe the surface chemistry evolution of PCN-0.5 during PMS activation for 4-CP degradation. FTIR spectra in Figure 4b depict significant characteristic adsorption peaks of PMS at 610 cm^{-1} (S−O) and 1107 cm^{-1} (S═O═S).[39] There was a blue-shift of 7 and 10 cm^{-1} for both peaks when PCN was mixed with PMS, indicating that the HO−O−SO_3^- structure of PMS bonded to and sulfonated the PCN surface.[56] The Raman spectra (Figure 4c) show that the characteristic peaks of SO_4^{2-} and HSO_5^- for PMS alone at 979 and 1093 cm^{-1},[57−59] respectively. A new peak appeared at 1146 cm^{-1} on the PCN-0.5 after adding PMS. This new peak is likely due to the active peroxo species (PMS*) bonding with the surface active sites of PCN-0.5. Furthermore, the HSO_5^- peak in PMS at 1093 cm^{-1} showed a red-shift of 12 cm^{-1} in the PCN-0.5/PMS systems, which may be attributed to the strong surface interaction between PMS and PCN-0.5 that changes the stretching vibration amplitude of HSO_5^-. Moreover, all the PMS and PMS* peaks in the range of Raman shifts from 950 to 1150 cm^{-1} (except for the SO_4^{2-} peak at 984 cm^{-1}) disappeared when 4-CP was added, suggesting that surface PCN-0.5-PMS active complexes were the dominant nonradical active species for 4-CP degradation.

https://dx.doi.org/10.1021/acs.est.0c03207
Environ. Sci. Technol. 2020, 54, 8473−8481

On the basis of the above analyses, a nonradical catalytic mechanism for the oxidative degradation of 4-CP in PCN-0.5/PMS system is inferred: PMS and 4-CP molecules are first absorbed on the surface of PCN-0.5; the interaction between PMS and PCN-0.5 can generate surface-bonding active complexes, which mediate electron transfer from the adsorbed 4-CP (electron donor) to PMS (electron acceptor) as illustrated in Scheme 1. This is corroborated by in situ

Scheme 1. Proposed Non-Radical Reaction Mechanism for PMS Activation by PCN-0.5

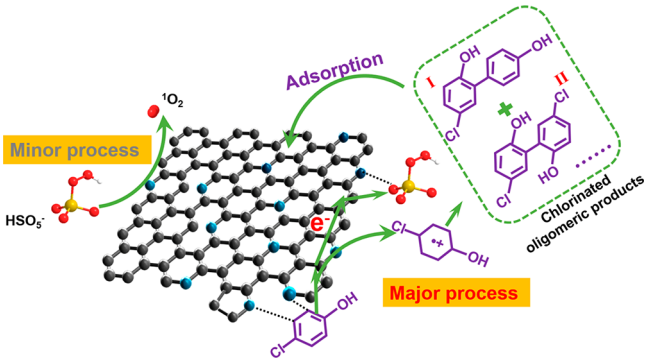

measurements of open circuit potential of surface PMS* on PCN-*x* catalysts (Figure 4d), which were monitored (Text S1) to reveal the formation of oxidative species in this nonradical based PMS activation process.[59] Open circuit potentials increased when PMS was added, indicating the formation of PCN-*x*-PMS complexes with enhanced oxidation power. Potentials changed more for PCN-0.5-PMS (0.35 V) than for PCN-1-PMS (0.26 V) and PCN-1.5-PMS (0.04 V). This is consistent with higher contents of nongraphitic N (pyridinic and pyrrolic N) in the catalysts, which enhances the interaction between PMS and PCN-*x* and accordingly promotes generation of more surface-active complexes. Subsequently, these active complexes can accept electrons from 4-CP, resulting in its oxidative degradation (Scheme 1).

PMS adsorption on PCN-*x* catalysts is presented in Figure S14a. Significant positive correlations between the PMS* potentials with PMS adsorption (Figure S14b) and *k* values for 4-CP degradation (Figure S14c) were observed. These results reveal that enhanced PMS adsorption facilitates the formation of surface PCN-0.5-PMS complexes, and accordingly expedites electron transfer from 4-CP to PMS during the degradation process.

The chromatograms in Figures S15 and S16 show that 4-CP can produce chlorinated oligomeric intermediates (such as dimeric products with m/z = 219.02 and 252.98). According to above mediated electron transfer mechanism, phenoxyl radicals in various resonance forms can be produced via one-electron oxidation of phenolic compounds in the carbon-persulfate system,[60−62] and serve as the precursors of the oligomeric intermediates. The oligomeric products can be generated through C−O and C−C coupling between chlorophenol radicals. The related transformation pathways of 4-CP are proposed as shown in Figure S17, and details of the polymeric products are presented in Text S3.

Although halogenated oligomeric intermediates may raise concerns about their potential toxicity,[61] they were mainly adsorbed on the PCN-0.5 surface (Figures S15a) and were barely dissolved in aqueous phase (Figures S15b). Occlusion of active sites by these products causes significant deactivation of PCN-0.5; only ∼8% and ∼5% of 4-CP was degraded after 15 min in the second and third run test (Figure S18), respectively. Herein, a facile post-treatment is performed to regenerate the used PCN by organic solvent extraction of oligomeric intermediates. The regenerated PCN-0.5 after the second run exhibited 100% removal of 4-CP within 8 min (Figure S18).

Furthermore, high catalytic performance of PCN-0.5 was observed in real water matrices (i.e., tap water and lake water), with 100% removal efficiency of 4-CP within 8 min (Figure S19), likely due to less susceptibility of this nonradical oxidative system to interference by background inorganic and organic matter.[53] Although heavy metals that might be present in complex wastewaters may adsorb and passivate active sites of carbon materials,[62] Cu^{2+} (up to 10 mg/L) had a negligible effect on 4-CP degradation in the PCN-0.5/PMS system (Figure S19b).

Environmental Implications. This study offers a promising strategy to synthesize N-doped carbon catalysts (PCN-*x*) with large SSA, high N content, and controllable N configurations, which was demonstrated to be an efficient metal-free heterogeneous catalyst for PMS activation and organic pollutant removal. Pyridinic N and pyrrolic N were the primary active sites in PCN catalysts, which also increased the affinity of PMS and organic pollutants for the PCN surface. The generated PCN−PMS complexes can mediate electron-transfer for direct oxidation of 4-CP without the needs of easily scavenged free radicals. The findings highlight the significant role of pyridinic and pyrrolic N species in carbon materials catalyzed-PMS activation, and the critical role of interaction between substrates and catalysts in this surface mediated nonradical reaction system. This work also suggests the strategy to rational design of efficient N-rich carbocatalysts for persulfate-based AOPs.

The oxidation of 4-CP through the nonradical pathway forms chlorinated oligomeric byproducts, which accumulated on the surface of the catalyst but did not dissolve in aqueous solution. Oligomerization in this nonradical oxidation process generally achieves water detoxification. Although the adsorption of these byproducts can result in deactivation of the carbocatalyst, removal of the adsorbed byproducts by organic solvent extraction can partially recover the used PCN catalysts, further insights are needed to regenerate N-rich carbocatalysts and make them more durable for practical applications in wastewater remediation.

■ ASSOCIATED CONTENT

Supporting Information

The Supporting Information is available free of charge at https://pubs.acs.org/doi/10.1021/acs.est.0c03207.

Texts S1, S3, and Figures S15−S17, characterization of catalysts and methods for intermediates detection during 4-CP oxidation; Text S2, activation evaluation; Table S1, HPLC conditions for different organic compounds; Tables S2−S6, Figures S1−S6, additional characterizations of catalysts; Figures S7 and S9−S14, additional catalytic tests; Figure S8, relationship between oxidation rates of 4-CP and contents of different N species or defects in as-prepared catalysts; Figures S18 and S19, recyclability tests and practical application of the catalysts (PDF)

https://dx.doi.org/10.1021/acs.est.0c03207
Environ. Sci. Technol. 2020, 54, 8473−8481

AUTHOR INFORMATION

Corresponding Author

Mingce Long − *School of Environmental Science and Engineering, Key Laboratory for Thin Film and Microfabrication of the Ministry of Education, Shanghai Jiao Tong University, Shanghai 200240, P. R. China;* orcid.org/0000-0002-5168-8330; Phone: 86-21-5474-7354; Email: long_mc@sjtu.edu.cn; Fax: 86-21-5474-0825

Authors

Jie Miao − *School of Environmental Science and Engineering, Key Laboratory for Thin Film and Microfabrication of the Ministry of Education, Shanghai Jiao Tong University, Shanghai 200240, P. R. China*

Wei Geng − *School of Environmental Science and Engineering, Key Laboratory for Thin Film and Microfabrication of the Ministry of Education, Shanghai Jiao Tong University, Shanghai 200240, P. R. China*

Pedro J. J. Alvarez − *Department of Civil and Environmental Engineering, Rice University, Houston, Texas 77005, United States;* orcid.org/0000-0002-6725-7199

Complete contact information is available at: https://pubs.acs.org/10.1021/acs.est.0c03207

Notes

The authors declare no competing financial interest.

ACKNOWLEDGMENTS

Financial supports from the National Natural Science Foundation of China (no. 21876108), the National Key Research and Development Program of China (no. 2017YFE0195800) and the NSF ERC on Nanotechnology-Enabled Water Treatment (no. EEC-1449500), Shanghai Postdoctoral Excellence Program (no. 2019160) are gratefully acknowledged. We gratefully acknowledge the support in FTIR and XPS measurements and valuable suggestions by Mrs. Xiaofang Hu of the Instrumental Analysis Center of School of Environmental Science and Engineering and Mrs. Xue Ding of the Instrumental Analysis Center, Shanghai Jiao Tong University.

REFERENCES

(1) Alvarez, P. J.; Chan, C. K.; Elimelech, M.; Halas, N. J.; Villagrán, D. Emerging opportunities for nanotechnology to enhance water security. *Nat. Nanotechnol.* **2018**, *13*, 634.

(2) Zhao, X.; An, Q. D.; Xiao, Z. Y.; Zhai, S. R.; Shi, Z. One-step preparation of Fe_xO_y/N-GN/CNTs heterojunctions as a peroxymonosulfate activator for relatively highly-efficient methylene blue degradation. *Chin. J. Catal.* **2018**, *39*, 1842−1853.

(3) Wang, J.; Wang, S. Activation of persulfate (PS) and peroxymonosulfate (PMS) and application for the degradation of emerging contaminants. *Chem. Eng. J.* **2018**, *334*, 1502−1517.

(4) Rastogi, A.; Al-Abed, S. R.; Dionysiou, D. D. Sulfate radical-based ferrous-peroxymonosulfate oxidative system for PCBs degradation in aqueous and sediment systems. *Appl. Catal., B* **2009**, *85* (3−4), 171−179.

(5) Duan, X.; Sun, H.; Wang, S. Metal-free carbocatalysis in advanced oxidation reactions. *Acc. Chem. Res.* **2018**, *51*, 678−687.

(6) Zhang, Y.; Pan, H.; Murugananthan, M.; Sun, P.; Dionysiou, D. D.; Zhang, K.; Khan, A.; Zhang, Y. Glucose and melamine derived nitrogen-doped carbonaceous catalyst for non-radical peroxymonosulfate activation process. *Carbon* **2020**, *156*, 399−409.

(7) Lee, H.; Kim, H.-i.; Weon, S.; Choi, W.; Hwang, Y. S.; Seo, J.; Lee, C.; Kim, J.-H. Activation of persulfates by graphitized nanodiamonds for removal of organic compounds. *Environ. Sci. Technol.* **2016**, *50*, 10134−10142.

(8) Sun, H.; Kwan, C.; Suvorova, A.; Ang, H. M.; Tadé, M. O.; Wang, S. Catalytic oxidation of organic pollutants on pristine and surface nitrogen-modified carbon nanotubes with sulfate radicals. *Appl. Catal., B* **2014**, *154*, 134−141.

(9) Duan, X.; Sun, H.; Wang, Y.; Kang, J.; Wang, S. N-doping-induced non-radical reaction on single- walled carbon nanotubes for catalytic phenol oxidation. *ACS Catal.* **2015**, *5*, 553−559.

(10) Cheng, X.; Guo, H.; Zhang, Y.; Wu, X.; Liu, Y. Non-photochemical production of singlet oxygen via activation of persulfate by carbon nanotubes. *Water Res.* **2017**, *113*, 80−88.

(11) Tang, L.; Liu, Y.; Wang, J.; Zeng, G.; Deng, Y.; Dong, H.; Feng, H.; Wang, J.; Peng, B. Enhanced activation process of persulfate by mesoporous carbon for degradation of aqueous organic pollutants: Electron transfer mechanism. *Appl. Catal., B* **2018**, *231*, 1−10.

(12) Novoselov, K. S.; Falko, V. I.; Colombo, L.; Gellert, P. R.; Schwab, M. G.; Kim, K. A roadmap for graphene. *Nature* **2012**, *490*, 192−200.

(13) Wu, D.; Song, W.; Chen, L.; Duan, X.; Xia, Q.; Fan, X.; Li, Y.; Zhang, F.; Peng, W.; Wang, S. High-performance porous graphene from synergetic nitrogen doping and physical activation for advanced non-radical oxidation. *J. Hazard. Mater.* **2020**, *381*, 121010.

(14) Restivo, J.; Rocha, R. P.; Silva, A. M.; Órfão, J. J.; Pereira, M. F.; Figueiredo, J. L. Catalytic performance of heteroatom-modified carbon nanotubes in advanced oxidation processes. *Chin. J. Catal.* **2014**, *35*, 896−905.

(15) Zhang, M.; Luo, R.; Wang, C.; Zhang, W.; Yan, X.; Sun, X.; Wang, L.; Li, J. Confined pyrolysis of metal-organic frameworks to N-doped hierarchical carbon for non-radical dominated advanced oxidation processes. *J. Mater. Chem. A* **2019**, *7*, 12547−12555.

(16) Duan, X.; Sun, H.; Wang, Y.; Kang, J.; Wang, S. N-doping-induced non-radical reaction on single-walled carbon nanotubes for catalytic phenol oxidation. *ACS Catal.* **2015**, *5*, 553−559.

(17) Wang, X.; Qin, Y.; Zhu, L.; Tang, H. Nitrogen-doped reduced graphene oxide as a bifunctional material for removing bisphenols: synergistic effect between adsorption and catalysis. *Environ. Sci. Technol.* **2015**, *49*, 6855−6864.

(18) Wang, J.; Duan, X.; Dong, Q.; Meng, F.; Tan, X.; Liu, S.; Wang, S. Facile synthesis of N-doped 3D graphene aerogel and its excellent performance in catalytic degradation of antibiotic contaminants in water. *Carbon* **2019**, *144*, 781−790.

(19) Duan, X.; Ao, Z.; Sun, H.; Indrawirawan, S.; Wang, Y.; Kang, J.; Liang, F.; Zhu, Z. H.; Wang, S. Nitrogen-doped graphene for generation and evolution of reactive radicals by metal-free catalysis. *ACS Appl. Mater. Interfaces* **2015**, *7*, 4169−4178.

(20) Chen, X.; Duan, X.; Oh, W.-D.; Zhang, P.-H.; Guan, C. T.; Zhu, Y. A.; Lim, T. T. Insights into nitrogen and boron-co-doped graphene toward high-performance peroxymonosulfate activation: Maneuverable NB bonding configurations and oxidation pathways. *Appl. Catal., B* **2019**, *253*, 419−432.

(21) Yang, H. B.; Miao, J.; Hung, S.-F.; Chen, J.; Tao, H. B.; Wang, X.; Zhang, L.; Chen, R.; Gao, J.; Chen, H. M.; et al. Identification of catalytic sites for oxygen reduction and oxygen evolution in N-doped graphene materials: Development of highly efficient metal-free bifunctional electrocatalyst. *Sci. Adv.* **2016**, *2*, No. e1501122.

(22) Ding, W.; Li, L.; Xiong, K.; Wang, Y.; Li, W.; Nie, Y.; Chen, S.; Qi, X.; Wei, Z. Shape fixing via salt recrystallization: a morphology-controlled approach to convert nanostructured polymer to carbon nanomaterial as a highly active catalyst for oxygen reduction reaction. *J. Am. Chem. Soc.* **2015**, *137*, 5414−5420.

(23) Li, X.; Huang, X.; Xi, S.; Miao, S.; Ding, J.; Cai, W.; Liu, S.; Yang, X.; Yang, H.; Gao, J.; et al. Single cobalt atoms anchored on porous N-doped graphene with dual reaction sites for efficient fenton-like catalysis. *J. Am. Chem. Soc.* **2018**, *140*, 12469−12475.

(24) Li, D.; Duan, X.; Sun, H.; Kang, J.; Zhang, H.; Tade, M. O.; Wang, S. Facile synthesis of nitrogen-doped graphene via low-temperature pyrolysis: the effects of precursors and annealing

ambience on metal-free catalytic oxidation. *Carbon* **2017**, *115*, 649−658.
(25) Chen, X.; Oh, W.-D.; Hu, Z. T.; Sun, Y.-M.; Webster, R. D.; Li, S. Z.; Lim, T. T. Enhancing sulfacetamide degradation by peroxymonosulfate activation with N-doped graphene produced through delicately-controlled nitrogen functionalization via tweaking thermal annealing processes. *Appl. Catal., B* **2018**, *225*, 243−257.
(26) Chen, X.; Oh, W. D.; Lim, T. T. Graphene- and CNTs-based carbocatalysts in persulfates activation: Material design and catalytic mechanisms. *Chem. Eng. J.* **2018**, *354*, 941−976.
(27) Liu, X.; Kang, J.; Dai, Y.; Dong, C.; Guo, X.; Jia, X. Graphene-like nitrogen-doped carbon nanosheet prepared from direct calcination of dopamine confined by g-C_3N_4 for oxygen reduction. *Adv. Mater. Interfaces* **2018**, *5*, 1800303.
(28) Yu, H.; Shang, L.; Bian, T.; Shi, R.; Waterhouse, G. I. N.; Zhao, Y.; Zhou, C.; Wu, L.-Z.; Tung, C.-H.; Zhang, T. Nitrogen-doped porous carbon nanosheets templated from g-C_3N_4 as metal-free electrocatalysts for efficient oxygen reduction reaction. *Adv. Mater.* **2016**, *28*, 5080−5086.
(29) Li, J.; Zhang, Y.; Zhang, X.; Han, J.; Wang, Y.; Gu, L.; Zhang, Z.; Wang, X.; Jian, J.; Xu, P.; Song, B. Direct transformation from graphitic C_3N_4 to nitrogen-doped graphene: An efficient metal-free electrocatalyst for oxygen reduction reaction. *ACS Appl. Mater. Interfaces* **2015**, *7*, 19626−19634.
(30) Han, C.; Meng, P.; Waclawik, E. R.; Zhang, C.; Li, X. H.; Yang, H.; Antonietti, M.; Xu, J. Palladium/graphitic carbon nitride (g-C_3N_4) stabilized emulsion microreactor as a store for hydrogen from ammonia borane for use in alkene hydrogenation. *Angew. Chem., Int. Ed.* **2018**, *57*, 14857−14861.
(31) Ong, W. J.; Tan, L. L.; Ng, Y. H.; Yong, S. T.; Chai, S. P. Graphitic carbon nitride (g-C_3N_4)-based photocatalysts for artificial photosynthesis and environmental remediation: are we a step closer to achieving sustainability? *Chem. Rev.* **2016**, *116*, 7159−7329.
(32) Qu, K.; Zheng, Y.; Dai, S.; Qiao, S. Z. Polydopamine-graphene oxide derived mesoporous carbon nanosheets for enhanced oxygen reduction. *Nanoscale* **2015**, *7*, 12598−12605.
(33) Liu, Y.; Ai, K.; Lu, L. Polydopamine and its derivative materials: synthesis and promising applications in energy, environmental, and biomedical fields. *Chem. Rev.* **2014**, *114*, 5057−115.
(34) Kong, J.; Shahabadi, S. I. S.; Lu, X. Integration of inorganic nanostructures with polydopamine-derived carbon: tunable morphologies and versatile applications. *Nanoscale* **2016**, *8*, 1770−1788.
(35) Hu, P.; Su, H.; Chen, Z.; Yu, C.; Li, Q.; Zhou, B.; Alvarez, P. J.; Long, M. Selective degradation of organic pollutants using an efficient metal-free catalyst derived from carbonized polypyrrole via peroxymonosulfate activation. *Environ. Sci. Technol.* **2017**, *51*, 11288−11296.
(36) Gao, Y.; Zhu, Y.; Lyu, L.; Zeng, Q.; Xing, X.; Hu, C. Electronic structure modulation of graphitic carbon nitride by oxygen doping for enhanced catalytic degradation of organic pollutants through peroxymonosulfate activation. *Environ. Sci. Technol.* **2018**, *52*, 14371−14380.
(37) Lin, Z.; Waller, G.; Liu, Y.; Liu, M.; Wong, C. P. Facile synthesis of nitrogen-doped graphene via pyrolysis of graphene oxide and urea, and its electrocatalytic activity toward the oxygen reduction reaction. *Adv. Energy Mater.* **2012**, *2*, 884−888.
(38) Liang, P.; Zhang, C.; Duan, X.; Sun, H.; Liu, S.; Tade, M. O.; Wang, S. N-doped graphene from metal-organic frameworks for catalytic oxidation of p-hydroxylbenzoic acid: N-functionality and mechanism. *ACS Sustainable Chem. Eng.* **2017**, *5*, 2693−2701.
(39) Wang, H.; Guo, W.; Liu, B.; Wu, Q.; Luo, H.; Zhao, Q.; Si, Q.; Sseguya, F.; Ren, N. Edge-nitrogenated biochar for efficient peroxydisulfate activation: An electron transfer mechanism. *Water Res.* **2019**, *160*, 405−414.
(40) Li, X.; Wang, H.; Robinson, J. T.; Sanchez, H.; Diankov, G.; Dai, H. Simultaneous nitrogen doping and reduction of graphene oxide. *J. Am. Chem. Soc.* **2009**, *131*, 15939−15944.
(41) Bai, X.; Shi, Y.; Guo, J.; Gao, L.; Wang, K.; Du, Y.; Ma, T. Catalytic activities enhanced by abundant structural defects and balanced N distribution of N-doped graphene in oxygen reduction reaction. *J. Power Sources* **2016**, *306*, 85−91.
(42) Guo, D.; Shibuya, R.; Akiba, C.; Saji, S.; Kondo, T.; Nakamura, J. Active sites of nitrogen-doped carbon materials for oxygen reduction reaction clarified using model catalysts. *Science* **2016**, *351*, 361−365.
(43) Xu, Y.; Mo, Y.; Tian, J.; Wang, P.; Yu, H.; Yu, J. The synergistic effect of graphitic N and pyrrolic N for the enhanced photocatalytic performance of nitrogen-doped graphene/TiO_2 nanocomposites. *Appl. Catal., B* **2016**, *181*, 810−817.
(44) Yin, R.; Guo, W.; Wang, H.; Du, J.; Wu, Q.; Chang, J.-S.; Ren, N. Singlet oxygen-dominated peroxydisulfate activation by sludge-derived biochar for sulfamethoxazole degradation through a non-radical oxidation pathway: Performance and mechanism. *Chem. Eng. J.* **2019**, *357*, 589−599.
(45) Zou, J. P.; Chen, Y.; Liu, S. S.; Xing, Q.-J.; Dong, W. H.; Luo, X. B.; Dai, W. L.; Xiao, X.; Luo, J. M.; Crittenden, J. Electrochemical oxidation and advanced oxidation processes using a 3D hexagonal Co_3O_4 array anode for 4-nitrophenol decomposition coupled with simultaneous CO_2 conversion to liquid fuels via a flower-like CuO cathode. *Water Res.* **2019**, *150*, 330−339.
(46) Indrawirawan, S.; Sun, H.; Duan, X.; Wang, S. Low temperature combustion synthesis of nitrogen-doped graphene for metal-free catalytic oxidation. *J. Mater. Chem. A* **2015**, *3*, 3432−3440.
(47) Liu, G.; Lv, H.; Sun, H.; Zhou, X. Fabrication of tubelike Co_3O_4 with superior peroxidase-like activity and activation of PMS by a facile electrospinning technique. *Ind. Eng. Chem. Res.* **2018**, *57*, 2396−2403.
(48) Radovic, L. R.; Moreno-Castilla, C.; Rivera-Utrilla, J. Carbon materials as adsorbents in aqueous solutions. *Chem. Phys. Carbon* **2001**, 227−406.
(49) Ko, S. O.; Jun, S. Y.; Lee, D. H.; Park, J.; Shin, W. S. Effects of oxidative coupling reaction of 4-chlorophenol with manganese oxide on the phenanthrene sorption. *J. Environ. Sci. Health, Part A: Toxic/Hazard. Subst. Environ. Eng.* **2007**, *42*, 257−263.
(50) Guan, Y. H.; Ma, J.; Ren, Y. M.; Liu, Y. L.; Xiao, J. Y.; Lin, L. Q.; Zhang, C. Efficient degradation of atrazine by magnetic porous copper ferrite catalyzed peroxymonosulfate oxidation via the formation of hydroxyl and sulfate radicals. *Water Res.* **2013**, *47*, 5431−5438.
(51) Miao, J.; Sunarso, J.; Su, C.; Zhou, W.; Wang, S.; Shao, Z. $SrCo_{1-x}Ti_xO_{3-\delta}$ perovskites as excellent catalysts for fast degradation of water contaminants in neutral and alkaline solutions. *Sci. Rep.* **2017**, *7*, 44215.
(52) Hu, P.; Long, M.; Bai, X.; Wang, C.; Cai, C.; Fu, J.; Zhou, B.; Zhou, Y. Monolithic cobalt-doped carbon aerogel for efficient catalytic activation of peroxymonosulfate in water. *J. Hazard. Mater.* **2017**, *332*, 195−204.
(53) Yun, E. T.; Lee, J. H.; Kim, J.; Park, H. D.; Lee, J. Identifying the non-radical mechanism in the peroxymonosulfate activation process: singlet oxygenation versus mediated electron transfer. *Environ. Sci. Technol.* **2018**, *52*, 7032−7042.
(54) Ho, S.-H.; Chen, Y.-d.; Li, R.; Zhang, C.; Ge, Y.; Cao, G.; Ma, M.; Duan, X.; Wang, S.; Ren, N.-q. N-doped graphitic biochars from C-phycocyanin extracted Spirulina residue for catalytic persulfate activation toward non-radical disinfection and organic oxidation. *Water Res.* **2019**, *159*, 77−86.
(55) Chen, C.; Li, F.; Chen, H.-L.; Kong, M. G. Interaction between air plasma-produced aqueous $^1O_2$ and the spin trap DMPO in electron spin resonance. *Phys. Plasmas* **2017**, *24*, 103501.
(56) Luo, R.; Li, M.; Wang, C.; Zhang, M.; Khan, M. A. N.; Sun, X.; Shen, J.; Han, W.; Wang, L.; Li, J. Singlet oxygen-dominated non-radical oxidation process for efficient degradation of bisphenol A under high salinity condition. *Water Res.* **2019**, *148*, 416−424.
(57) Zhang, T.; Zhu, H.; Croue, J. P. Production of sulfate radical from peroxymonosulfate induced by a magnetically separable $CuFe_2O_4$ spinel in water: Efficiency, stability, and mechanism. *Environ. Sci. Technol.* **2013**, *47*, 2784−2791.

https://dx.doi.org/10.1021/acs.est.0c03207
Environ. Sci. Technol. 2020, 54, 8473−8481

(58) Ren, Y.; Lin, L.; Ma, J.; Yang, J.; Feng, J.; Fan, Z. Sulfate radicals induced from peroxymonosulfate by magnetic ferrospinel MFe_2O_4 (M = Co, Cu, Mn, and Zn) as heterogeneous catalysts in the water. *Appl. Catal., B* **2015**, *165*, 572−578.
(59) Ren, W.; Nie, G.; Zhou, P.; Zhang, H.; Duan, X.; Wang, S. The intrinsic nature of persulfate activation and N-doping in carbocatalysis. *Environ. Sci. Technol.* **2020**, *54*, 6438.
(60) Su, H.; Wei, Y.; Qu, X.; Yu, C.; Li, Q.; Alvarez, P. J.; Long, M. Mechanistic inference on the reaction kinetics of phenols and anilines in carbon nanotubes-activated peroxydisulfate systems: pp-LFERs and QSARs analyses. *Chem. Eng. J.* **2020**, *385*, 123923.
(61) Guan, C.; Jiang, J.; Pang, S.; Luo, C.; Ma, J.; Zhou, Y.; Yang, Y. Oxidation kinetics of bromophenols by non-radical activation of peroxydisulfate in the presence of carbon nanotube and formation of brominated polymeric products. *Environ. Sci. Technol.* **2017**, *51*, 10718−10728.
(62) Wang, J.; Yang, Q.; Yang, W.; Pei, H.; Zhang, L.; Zhang, T.; Hu, N.; Suo, Y.; Wang, J. Adsorptive catalysis of hierarchical porous heteroatom-doped biomass: from recovered heavy metal to efficient pollutant decontamination. *J. Mater. Chem. A* **2018**, *6* (34), 16690−16698.

https://dx.doi.org/10.1021/acs.est.0c03207
Environ. Sci. Technol. 2020, 54, 8473−8481